Design and Analysis of a Permanent Magnet Claw Pole/Transverse Flux Motor with SMC Core

YouGuang GUO, Jian Guo ZHU, and Haiwei LU
Center for Electrical Machines and Power Electronics, Faculty of Engineering
University of Technology, Sydney
Sydney, Australia

***Abstract*—This paper presents the design and analysis of a claw pole/transverse flux motor (CPTFM) with soft magnetic composite (SMC) core and permanent magnet flux-concentrating rotor. Three-dimensional magnetic field finite element analysis is conducted to accurately calculate key motor parameters such as winding flux, back electromotive force, winding inductance, and core loss. Equivalent electric circuit is derived under optimum brushless DC control condition for motor performance prediction, and computer search techniques are applied for design optimization. All these computations and analyses have been implemented in a commercial software ANSYS for development of the SMC CPTFM prototype.**

Keywords-claw pole/transverse flux motor, core loss, finite element analysis, inductance, soft magnetic composite.

I. INTRODUCTION

Permanent magnet (PM) machines with transverse flux structure have attracted strong interest of research since Weh and May proposed the concept of transverse flux machine (TFM) in 1986 [1]. TFMs can produce very large torque to volume ratio provided that the number of poles is big, and hence naturally they are suitable for direct drive applications, which require high torque at low speed.

The feature of high specific torque is particularly true for the double-sided, flux-concentrating structure, but all the double-sided designs reported are considered to be too complicated to manufacture [2]. Single-sided structure is much simpler but the power factor is very low, typically 0.35, due to the very large flux leakage [3]. To overcome these problems, a large amount of work has been performed by various researchers and a notable example is the claw pole/transverse flux motor (CPTFM) [4]. The CPTFM structure features both the simplicity of the single-sided TFM and the high performance of the double-sided one [5]. In order to increase the power factor, the overlap of adjacent claw poles is shortened to reduce the flux leakage between the side surfaces. The decrease of the axial length of claw poles will not necessarily reduce the main flux of the stator winding produced by the rotor permanent magnets (PMs) if the flux-concentrating structure is employed.

In a CPTFM, the magnetic field is substantially three-dimensional (3D) and this makes the lamination of the core is very difficult. Soft magnetic composite (SMC) materials offer an ideal solution thanks to their unique properties, such as magnetic and thermal isotropy, very low eddy current loss and relatively low total core loss, net-shape fabrication process with good tolerance and surface smooth (no need of further machining), and prospect of low cost mass production [6, 7]. The basis of SMC materials is the bonded iron powder of high purity and compressibility. The powder particles are coated with an organic material, which produces an electrical insulation between particles. The coated powder is compressed in a die into a solid with the desired shape and dimensions, and the solid is then heat treated and annealed to cure the bond [8].

SMC materials are generally magnetically isotropic due to the powdered nature, and this creates key design benefits for electromagnetic devices. Radically different topologies can be explored to achieve high performance as the designers can now ignore the restraints imposed by the lamination technology, e.g. that the magnetic field must flow within the lamination plane to avoid excessive eddy current loss. Typical examples of SMC application are the machines with three-dimensional (3D) flux path [9]. In such machines, due to 3D magnetic field, the core construction using electrical steels is very difficult or almost impossible.

Because the iron particles are insulated by the surface coating and adhesive, which is used for composite bonding, the eddy current loss is much lower than that in laminated steels, especially at higher frequencies. The total loss is dominated by hysteresis loss, which is higher than that of laminated steels due to the particle deformation during compaction. This property implies SMC motors to be better operated at higher frequencies, resulting in reduced machine size and weight.

Besides the above unique properties, SMC materials have some outstanding disadvantages that should be carefully considered, such as lower magnetic permeability and lower saturation flux density compared with lamination steels. A direct replacement for electrical sheets by SMC will result in poorer machine performance. Therefore, it is important to avoid the disadvantages when exploiting the advantages at various stages such as design, manufacturing and application. For example, SMC material would be appropriate for construction of PM motors for which the magnetic reluctance of the magnet dominates the magnetic circuit, making such motors insensitive to the permeability of the core.

This paper presents the design and analysis of a three-phase three-stack CPTFM with SMC core and PM flux-concentrating

rotor. 3D finite element analysis (FEA) of magnetic field is carried out for determining key motor parameters, such as back electromotive force (*emf*), winding inductance, and core losses. The motor performance is predicted by an equivalent circuit with the condition of the optimum brushless DC control. The analysis method has been validated by two other SMC motor prototypes with similar structures, i.e. a claw pole motor and a TFM.

II. CLAW POLE/TRANSVERSE FLUX MOTOR

Fig. 1 illustrates the layout and FEA solution region of one pole-pitch of one stack of a CPTFM, and Table I lists the major dimensions and parameters. Both the stator core and the rotor PM flux-concentrating iron use SOMALOY™ 500 [10], an SMC material specially developed for electrical machine application by Höganäs AB, Sweden. The SMC material has a maximum flux density of 2.1 T at 100 kA/m, a remanence of 0.25 T, a coercive force of 250 A/m, an electrical resistivity of 30 μΩm, a thermal conductivity of 17 W/(m·K), and an initial relativity permeability of 130.

A simple concentrated winding per phase is enclosed by two SMC claw pole discs, which can be readily made by mold compaction. The magnetic fluxes produced by two adjacent rotor NdFeB permanent magnets flow circumferentially into the iron part between them (in the figure, only one magnet is shown for the one pole pitch model while the main magnetic circuit has the lowest reluctance). The fluxes aid each other and then flow axially and radially into the claw pole via the airgap. Three phases are stacked axially with the stator cores shifted by 120° electrical and the rotor PMs aligned.

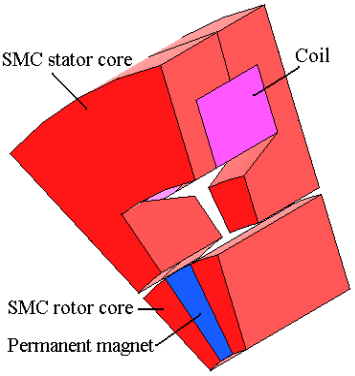

Figure 1. Layout and FEA solution region of a CPTFM

TABLE I. MAJOR DIMENSIONS AND PARAMETERS OF THE CPTFM

Parameters and Dimensions	Value
Rated power (W)	2200
Rated speed (rpm)	3000
Rated frequency (Hz)	300
Number of poles	12
Number of phases	3
Stator core outer diameter (mm)	110
Middle airgap diameter (mm)	56.5
Airgap length (mm)	1
Magnet height (mm)	14
Stack axial length (mm)	34
Claw pole overlap ratio (%)	30
Coil window dimension (mm^2)	20 x 10

III. 3D FEA OF MAGNETIC FIELD

A. FEA Solution Region and No-load Field Distribution

Because of the complex geometry, the magnetic field in a CPTFM is truly 3D. The armature carries significant field in all three directions. This is only achievable using SMC material. Consequently, for the correct calculation of magnetic field and motor characteristics, a 3D numerical analysis, e.g. FEA, is required. FEA has been considered as a suitable and accurate method of field computation to aid motor design, allowing material non-linearity and structure details to be included.

Because of the magnetic independence between stacks and the symmetry of the motor structure, it is only required to analyze the magnetic field in one pole-pitch region of one phase, as shown in Fig. 1. At the two radial boundary planes, the magnetic scalar potential used to solve the magnetic field distribution should obey the so-called half-periodical boundary conditions:

$$\varphi_m\left(r, \Delta\theta/2, z\right) = -\varphi_m\left(r, -\Delta\theta/2, -z\right) \tag{1}$$

where $\Delta\theta = 30^o$ is the angle of one pole pitch. The original point of the cylindrical coordinate is located at the center of the stack. The conditions of the magnetic flux density on the two radial boundary planes are:

$$B_{r,\theta}(r, \Delta\theta/2, z) = -B_{r,\theta}(r, -\Delta\theta/2, -z) \tag{2}$$

$$B_z(r, \Delta\theta/2, z) = B_z(r, -\Delta\theta/2, -z) \tag{3}$$

Fig. 2 shows the no-load magnetic field distribution when the main magnetic circuit has the highest permeability and the stator winding links the maximum magnetic flux. It can be found that the major path for the magnetic flux of the permanent magnet is along the north pole of PM – the rotor flux-concentrating iron between two PMs – the main air gap – one of the composite claw pole stator core pieces – the stator yoke – another composite claw pole stator core piece – main airgap – another rotor flux-concentrating iron, – then the south pole of PM to form a closed loop. There is also a considerable amount of leakage flux through the gaps between the side and end surfaces of the claw poles of the two separated pieces.

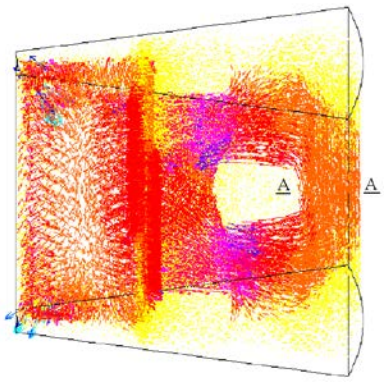

Figure 2. No-load flux density vector plots

B. *PM Flux and Back emf*

A number of key parameters of the motor can be determined from the numerical magnetic field analysis. The no-load magnetic field distribution is calculated to find out the magnetic flux linking the stator winding, as shown in Fig. 3. For the CPTFM, the curve of the PM flux, defined as the winding flux produced by the rotor PMs, against rotor angle is found to be closely sinusoidal. The induced back *emf* under rotation is inferred by differentiating the no-load flux linkage with respect to rotor angle.

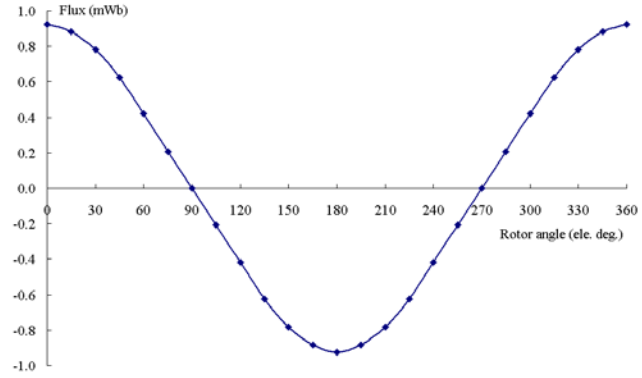

Figure 3. Per-turn PM flux against rotor angle

C. *Winding Inductance*

The inductance of the winding is one of the key parameters determining the motor performance. Because the magnetic circuit of each stack is almost independent, the mutual inductance between the three phase windings can be considered as zero. The self-inductance of one phase winding can be calculated by the two conventional approaches, i.e. the flux-linkage method as

$$L = \frac{\lambda}{i} = \frac{N\phi}{i} \tag{4}$$

or the energy method as

$$L = \frac{2W_c}{i^2} \tag{5}$$

where λ, ϕ and W_c are the magnitudes of the flux-linkage and flux linking the winding, and the magnetic co-energy stored in the whole machine, respectively, produced by a current i in each of N turns. The flux and magnetic co-energy can be obtained from the results of a field analysis with a current i while the PMs are "switched off", i.e. remanence is set to zero.

A difficulty with the flux-linkage method is the accurate determination of the flux flowing through the stator winding. Theoretically, the flux can be computed by the surface integral of flux density $\boldsymbol{B}$, or the loop integral of vector potential $\boldsymbol{A}$ after the magnetic field distribution is solved by FEA, but it is not easy to define a proper integration surface or path when the winding is not a simple loop and is of non-negligible size. For this CPTFM motor, the winding flux can be approximately calculated based on the middle cross-sectional area of the stator yoke, marked as A-A in Fig. 2.

By contrast, the energy method can avoid the difficulty of choosing the proper integration geometry. It calculates the energy or co-energy stored in all the elements and is considered as quite accurate because the principle of FEA is based on the minimization of magnetic field energy. In this paper, the investigation on the winding inductance is mainly carried out by the energy method.

To consider the saturation caused by both the stator current and PMs, two-step analyses are carried out, i.e. a non-linear analysis with the excitations of both PMs and armature current i for saving the permeability of each element, and then a linear analysis with a stator current only and the saved permeabilities is performed to find the ϕ in (4) or the W_c in (5).

Under the condition of the optimum brushless DC control, the stator current is in phase with the back *emf*, i.e. lagging the PM flux by 90 degrees electrical. The fundamental of the stator current can be determined by

$$i = \sqrt{2} I_{rms} \sin\theta \tag{6}$$

where I_{rms} is the *rms* value of the stator current, θ is the rotor angle with the zero position where the claw poles line up with the rotor PM flux-concentrating irons, as shown in Fig. 1.

The calculated phase winding inductance (L_{sec}) versus different rotor angle and load is shown in Fig. 4. This calculation is in fact the secant (or apparent) inductance, i.e. the slope of the linearised characteristic of flux-linkage versus current through the origin and the operating point, as shown in Fig. 5.

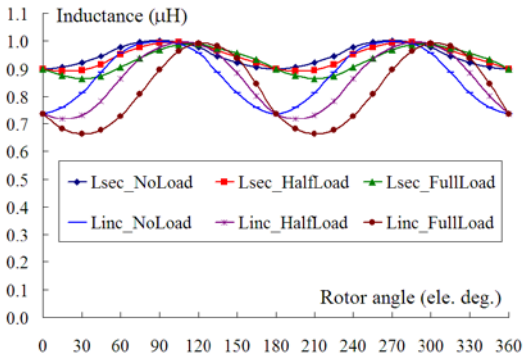

Figure 4. Calculated secant and incremental self-inductance of one turn of the phase winding

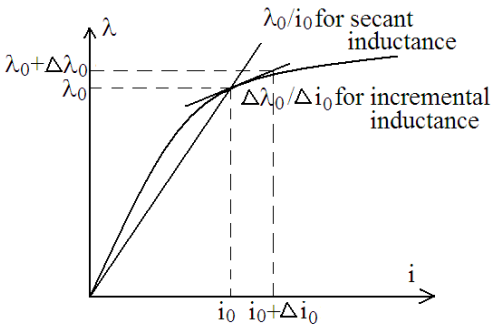

Figure 5. Curve of flux-linkage versus current

However, the behavior of an electric circuit is governed by the so-called incremental (or differential) inductance, along the tangential line at the operating point, as illustrated in Fig. 5. The calculation of the incremental inductance involves calculating the increment of flux-linkage due to a small perturbation of current. To avoid the difficulty in defining the integration geometry for flux-linkage computation, the incremental energy method (IEM) is often used [11, 12]. IEM computes the inductance using the magnetic field FEA in conjunction with energy/current perturbation. The general formulation of incremental self-inductance using the energy/current perturbation method is

$$L_{inc} = \frac{\partial \lambda}{\partial i} = \frac{\partial^2 W_c}{\partial i^2} \approx \frac{W_c(i+\Delta i) + W_c(i-\Delta i) - 2W_c(i)}{(\Delta i)^2} \tag{7}$$

It seems that two incremental analyses are required for self-inductance (and four for mutual ones) [13]. In fact, (7) can be reduced to a very simple form, requiring one incremental analysis only.

For linear analysis, the stator current i can be any value, i.e. 0. With a current perturbation Δi only (from zero current), this formula can be reduced to

$$L_{inc} \approx \frac{2\Delta W_c}{(\Delta i)^2} \tag{8}$$

where ΔW_c is the increment of magnetic co-energy, which equals the energy in the linear analysis.

In summary, the modified IEM calculates the incremental inductance by the following steps [14]: (I) Perform non-linear magnetic field analysis with the excitation of both the stator current and PMs; (II) Determine and save the differential permeability in each element; (III) Conduct linear analysis with the saved differential permeabilities and a perturbed current only; (IV) Calculate the co-energy increment and then the incremental inductance by (8). In fact, the perturbed current in (III) can be large since the magnetic field analysis is linear.

The computed incremental inductance of phase winding with different rotor angle and load is also shown in Fig. 4. It is noted that the incremental inductances are generally smaller than the secant ones. This is coincident with the slopes of the straight line through the operation point and the origin, and the tangential line at the operating point, as shown in Fig. 5. The inductance data could provide useful information for the design of high performance control scheme.

D. Core Losses

Core loss prediction is a key issue in motor design and performance analysis. It has been known that core losses are caused by not only alternating but also rotating magnetic fields, and core losses caused by different patterns are very different [15]. In the CPTFM, when the rotor rotates, the flux density locus at a certain location can be alternating (one-dimensional), circularly or elliptically rotating within a two-dimensional plane which may not be parallel to any axis, or even an irregular loop in a real 3D space, all with or without harmonics. As an example, Fig. 6 plots the computed flux density locus in the middle of the flux- concentrating iron. The magnetic field in the CPTFM is really complex with irregular 3D patterns.

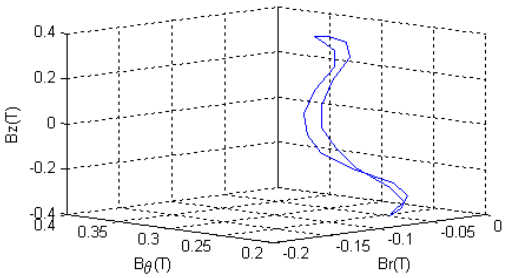

Figure 6. Flux density locus in a typical element in the rotor iron

An improved method is applied for predicting the core losses of this 3D-flux SMC motor [16]. Different formulations are used for core loss prediction with alternating, circular rotating, and elliptically rotating flux density vectors, respectively. For example, the alternating core loss is modeled by

$$P_a = C_{ha} f B_P{}^h + C_{ea} (f B_P)^2 + C_{aa} (f B_P)^{1.5} \tag{9}$$

and the core loss with circular flux by

$$P_a = C_{ha} f B_P{}^h + C_{ea} (f B_P)^2 + C_{aa} (f B_P)^{1.5} \tag{10}$$

where

$$\frac{P_{hr}}{f} = a_1 \left[\frac{1/s}{(a_2 + 1/s)^2 + a_3^2} - \frac{1/(2-s)}{[a_2 + 1/(2-s)]^2 + a_3^2} \right] \tag{11}$$

$$s = 1 - \frac{B_P}{B_s} \sqrt{1 - \frac{1}{a_2^2 + a_3^2}} \tag{12}$$

The coefficients C_{ha}, h, C_{ea}, C_{aa}, C_{er}, C_{ar}, a_1, a_2, a_3 and B_s can be derived from the measured core losses on the cubic sample under various frequencies, f, and various peak flux densities, B_p by curve fitting techniques [15].

The core loss with elliptical $\boldsymbol{B}$ can be predicted from the alternating and circularly rotating core losses by

$$P_t = R_B P_r + (1 - R_B)^2 P_a \tag{13}$$

where $R_B = B_{min}/B_{maj}$ is the axis ratio of $\boldsymbol{B}$, B_{maj} and B_{min} are the major and minor axes of the elliptical $\boldsymbol{B}$ locus, P_r and P_a are the core losses with a circular $\boldsymbol{B}$ with $B_{maj}=B_{min}=B_p$ and an alternating $\boldsymbol{B}$ with peak value B_p.

In a rotating machine, the total core loss is the sum of the core losses in all elements. For any $\boldsymbol{B}$ locus in 3D space, its 3 components can be expended into Fourier series as

$$B_i(t) = \sum_{k=0}^{\infty} [B_{isk} \sin(2\pi k f t) + B_{ick} \cos(2\pi k f t)] \tag{14}$$

where $i = r, \theta, z$, B_r, B_θ, and B_z are the radial, circumferential and axial components of $\boldsymbol{B}$, respectively. Each of these harmonics consists of two parts:

$$\mathbf{n}_{sk}\sqrt{B_{rsk}{}^2+B_{\theta sk}{}^2+B_{zsk}{}^2}\sin(2\pi kft) \quad (15a)$$

$$\mathbf{n}_{ck}\sqrt{B_{rck}{}^2+B_{\theta ck}{}^2+B_{zck}{}^2}\cos(2\pi kft) \quad (15b)$$

where $\boldsymbol{n}_{sk}$ and $\boldsymbol{n}_{ck}$ are unit vectors, determined by B_{rsk}, $B_{\theta sk}$ and B_{zsk}, and B_{rck}, $B_{\theta ck}$ and B_{zck}, respectively. The two parts generally form an elliptical trajectory in a plane determined by $\boldsymbol{n}_{sk}$ and $\boldsymbol{n}_{ck}$. The major axis B_{kmaj} and the minor axis B_{kmin} can be obtained by a coordinate rotation for the standard equation.

The total loss in an element can be obtained by summing up the contributions from these flux density harmonics. For each elliptically rotating flux density harmonic, the loss can be predicted from the corresponding alternating and rotational losses according to the axis ratio of the elliptical flux density. Therefore, the total loss is

$$P_t=\sum_{k=0}^{\infty}\left[P_{rk}R_{BK}+(1-R_{BK})^2P_{ak}\right] \quad (16)$$

where $R_{BK}=B_{kmin}/B_{kmaj}$ is the axis ratio of the k-th harmonic flux density, P_{rk} is the purely rotational loss with flux density B_{kmaj}, and P_{ak} is the alternating loss with $B_p=B_{kmaj}$.

Fig. 7 shows the calculated core losses in the CPTFM at different speeds. Unlike conventional machines in which the copper loss dominates, SMC motors have comparable core and copper losses. It is an interesting design point that the two losses take the same value for high motor efficiency.

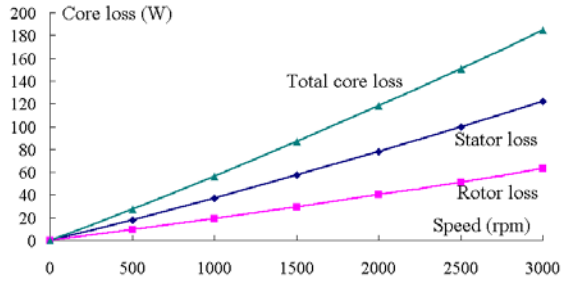

Figure 7. Calculated core losses against rotor speed

IV. Performance Prediction

The motor can be operated with a brushless DC drive scheme. Under the optimum control condition, the current I_1 is in phase with the back *emf*, E_1, in the stator winding and an equivalent electric circuit is shown in Fig. 8, where R_1 and X_1 are the resistance and synchronous reactance per phase, respectively.

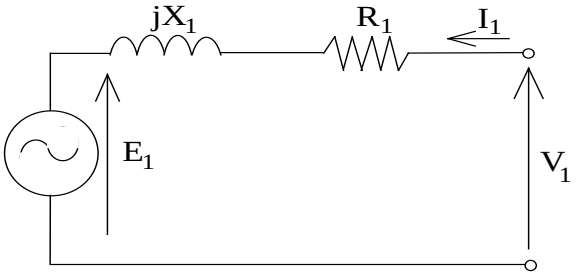

Figure 8. Equivalent electric circuit model of the CPTFM

The achievable maximum electromagnetic power P_{em} is

$$P_{em}=3E_1I_1 \quad (17)$$

The output power P_{out}, output torque T_{out}, input power P_{in} and efficiency η of the total drive system can be calculated by

$$P_{out}=P_{em}-P_{Fe}-P_{mec} \quad (18)$$

$$T_{out}=P_{out}/\omega_r \quad (19)$$

$$P_{in}=P_{em}+P_{inv}+P_{cu} \quad (20)$$

$$P_{cu}=3I_1{}^2R_1 \quad (21)$$

$$\eta=P_{out}/P_{in} \quad (22)$$

where P_{Fe} is the core loss, P_{mec} the mechanical loss, P_{inv} the inverter conduction loss, P_{cu} the copper loss, and ω_r the rotor angular speed in mechanical rad/s.

V. Motor Prototype

An optimization routine for the design of the CPTFM with SMC core has been set up, which includes three magnetic field FEAs for calculation of back *emf*, stator winding inductance and core loss. The magnetic field FEAs, thermal analysis, performance calculation, and optimization searches are all implemented in a commercial comprehensive software package, ANSYS. The designed SMC CPTFM is being constructed at the workshop, and will be tested and compared with the theoretical calculation.

The design and analysis method is similar to that for a claw pole and a transverse flux motors with SMC core, which has been validated by the substantial agreement between the theoretical calculation and experimental results on the two SMC motors [17].

VI. Discussion

The application of SMC materials in electrical machines, especially 3D flux PM machines, has a great potential and may lead to a revolution in the electrical machine manufacturing industry. In this paper, a claw pole transverse flux motor with SMC core is investigated based on our previous experiences on a claw pole and a transverse flux SMC motors.

Successful experiences have been achieved with the 3D flux design freedom, novel motor structures, and new fabrication techniques. The difficulties include low magnetic permeability, higher hysteresis loss, and weak mechanical strength, etc.

For commercial success of SMC machines, further work is required on development of optimum material composition, novel motor structures, advanced design and optimization methods, and practical manufacturing techniques using compaction/injection molding in close collaboration with industry.

Acknowledgment

The authors wish to thank Höganäs AB, Sweden, for supplying preforms of SOMALOY™ 500.

REFERENCES

[1] H. Weh and H. May, "Achievable force densities for permanent magnet excited machines in new configuration," in Proc. Int. Conf. on Electrical Machines, Munich, Germany, 1986, pp. 1107-1111.

[2] G. Henneberger and M. Bork, "Development of a new transverse flux motor," in Proc. IEE Colloq. New Topologies for PM Machine, June 1997, London, UK, pp. 1/1-6.

[3] M.R. Harris, G.H. Pajooman, and S.M. Abu Sharkh, "The problem of power factor in VRPM (transverse flux) machines," in Proc. IEE Electric Machines and Drives Conf., Cambridge, UK, 1997, pp. 386-390.

[4] C.P. Maddison, B.C. Mecrow, and A.G. Jack, "Claw pole geometries for high performance transverse flux machines," in Proc. Int. Conf. on Electrical Machines, Istanbul, Turkey, 1998, pp. 340-345.

[5] A. Masmoudi, A. Njeh, A. Mansouri, H. Trabelsi, and A. Elantably, "Optimizing the overlap between the stator teeth of a claw pole transverse-flux permanent-magnet machine," IEEE Trans. Magn., vol. 40, May 2004, pp. 1573-1578.

[6] "The latest development in soft magnetic composite technology," SMC Update, Reports of Höganäs AB, Sweden, 1997-2005. Available at http://www.hoganas.com/, see News then SMC Update.

[7] A.G. Jack, "Experience with the use of soft magnetic composites in electrical machines," in Proc. Int. Conf. on Electrical Machines, Istanbul, Turkey, Sept. 1998, pp. 1441-1448.

[8] M. Persson, P. Jansson, A.G. Jack, and B.C. Mecrow, "Soft magnetic composite materials – use for electrical machines," in Proc. 7th IEE Conf. on Electrical Machines and Drives, Durham, England, Sept. 1995, pp. 242-246.

[9] Y.G. Guo, J.G. Zhu, P.A. Watterson, and W. Wu, "Comparative study of 3-D flux electrical machines with soft magnetic composite core," IEEE Trans. Industry Applications, vol. 39, 2003, pp. 1696-1703.

[10] "Soft magnetic composites from Hoganas Metal Powders - SOMALOY™ 500," Hoganas Product Guide, 1997.

[11] N.A. Demerdash and T.W. Nehl, "Electrical machinery parameters and torques by current and energy perturbations from field computations – Part I: theory and formulation," IEEE Trans. Energy Conversion, vol. 14, 1999, pp. 1507-1513.

[12] N.A. Demerdash and T.W. Nehl, "Electrical machinery parameters and torques by current and energy perturbations from field computations – Part II: applications and results," IEEE Trans. Energy Conversion, vol. 14, 1999, pp. 1514-1522.

[13] M. Gyimesi and D. Ostergaard, "Inductance computation by incremental finite element analysis," IEEE Trans. Magn., vol. 35, 1999, pp. 1119-1122.

[14] Y.G. Guo, J.G. Zhu, H.W. Lu, R. Chandru, S.H. Wang, and J.X. Jin, "Determination of winding inductance in a claw pole permanent magnet motor with soft magnetic composite core," in Proc. Australasian Universities Power Eng. Conf., Hobart, Australia, Sept. 2005.

[15] Y.G. Guo, J.G. Zhu, J.J. Zhong, and W. Wu, "Core losses in claw pole permanent magnet machines with soft magnetic composite core," IEEE Trans. Magn., vol. 39, Sept. 2003, pp. 3199-3201.

[16] Y.G. Guo, J.G. Zhu, Z.W. Lin, and J.J. Zhong, "Measurement and modeling of core losses of soft magnetic composites under 3D magnetic excitations in rotating motors," IEEE Trans. Magn., vol. 41, Oct. 2005.

[17] J.G. Zhu and Y.G. Guo, "Study with magnetic property measurement of soft magnetic composite material and its application in electrical machines," in Proc. IEEE Ind. Applicat. Society Annual Meeting, Seattle, USA, Oct. 2004, pp. 373-380.